UCRL-CR--104380

DE90 015602

Final Report for the Tunable Driver for the LLNL FEL Experiment (Contract No. 2698003)

by

W.C. Guss, M.A. Basten, K.E. Kreischer, and R.J. Temkin

Plasma Fusion Center
Massachusetts Institute of Technology
Cambridge, MA 02139

This report describes main activities undertaken during the period 1 October 1988 to 30 September 1989 by MIT to support the Lawrence Livermore National Laboratory tunable FEL driver project. These activities are the design and construction of a gyrotron backward wave oscillator, and its operation. These activities were largely successful. The backward wave was generated and measurements of the voltage tunability made. Backward wave emitted powers were small resulting in efficiencies $\leq .5\%$.

The folowing report is divided into two sections, desribing the results obtained during the six month period of the contract, and the present status of the work.

Gyro-BWO Experiment Final Report

by

W.C. Guss, M.A. Basten, K.E. Kreischer, and R.J. Temkin

Summary

This section of the report covers the recent operation of the prototype backward-wave oscillator (BWO) gyrotron. The tube was mounted in its fixture on the superconducting magnet, the beam aligned, and microwaves generated. Initial alignment and operation was performed at low wiggler magnet strength ($B_w = 9\ G$) and thus low $\alpha = v_\perp / v_{||}$. The microwaves observed under these conditions were at a frequency just above the electron cyclotron frequency of the interaction region. Identification of these waves is tentatively that of forward waves generated in what is a very long gyrotron cavity. By increasing the wiggler field to $\approx 18\ G$, the backward wave could then be observed. Voltage tunability of the backward wave was demonstrated and frequencies from 133 GHz to 143 GHz were observed.

Introduction

Last year, MIT designed and constructed a driver for the FEL which was to provide electron cyclotron heating for the MTX tokomak. A backward wave oscillator (BWO) gyrotron was selected as the driver because of its fast continuous voltage tuning properties and because it would provide sufficient power ($\approx 10\ kW$). A design was completed for a BWO gyrotron to operate in the TE_{12} mode in the range $130-140\ GHz$. Parts were fabricated at MIT with the exception of the Pierce-wiggler gun which was being designed and constructed[1] by Varian Assoc., Inc. At the beginning of the current reporting period, the gun was received and construction completed. However because of delays in delivery of the gun, experimental work did not commence during the report period. Results of the design are included below. By necessity, computational tools guided the design and their results are included in this discussion. In addition, they were used to model the anticipated behavior of the device and some of those results will also be described.

Other BWO gyrotron experiments have been constructed and tested[2], successfully demonstrating voltage tunability and significant power generation in a fundamental rectangular cavity using a magnetron injection gun source. The present design has some novel features in that it uses an overmoded cylindrical cavity for operation at a much higher frequency ($130-140\ GHz$), a wide bandpass window, and a solid beam from a Pierce-wiggler type gun.

The goals of the present experimental program are to demonstrate the stable operation in the desired mode, to determine the tuning bandwidth, and to measure the efficiency over that range of frequencies. Operation will be tested for various values of the wiggler pitch and $\alpha(=v_\perp/v_\parallel)$. Another goal is to compare the experimental results to the computational predictions to benchmark the code. More accurate computational results can then be expected for future BWO gyrotron designs. Also, the suitability of the motheye window for broadband use will be studied.

Design Results

The backward wave gyrotron system is shown in Fig. 1. The Pierce gun successfully operated at 4 A and $60-70\ kV$. Although some beam in-

terception was observed, the fraction of beam current reaching the collector was $60 - 90\%$.

The Pierce gun includes a magnetic circuit to isolate the gun cathode from the fringe field of the superconducting magnet. Decoupling the two systems allows independent adjustment of the wiggler axial fields and the cavity field. The gun was dismounted from the wrap-on magnet and a magnetic probe inserted along the axis of the superconductor and wrap-on magnets. Figure 2 shows the resulting axial magnetic near the entrance to the wrap-on magnet. The wrap-on magnet position was adjusted so that there were no flux-tube pinching near the wrap-on magnet aperature. Additional measurements were made to locate the magnetic axis to facilitate the radial positioning of the Pierce gun. Without the gun system, the magnetic axis is roughly along the warm bore of the superconducting magnet, however, with the gun in place the magnetic axis was moved a significant distance. We suspect that inhomogeneities in the magnetic circuit of the gun are the cause. The magnetic circuit consists of a shroud around the coils of the wrap-on magnet, and a large plate between the superconducting magnet and the wrap-on magnet. Difficulties in beam alignment resulted from this field perturbation.

The transverse wiggler field was produced by winding multiple layers of permanent magnet strip on a stainless steel form which allowed removal from within the wrap-on magnet, and adjustment without breaking vacuum. For the initial stages of beam alignment, small beam size was desired so only two layers were used. The resulting transverse field is shown in Fig. 3 for two layers of magnetic strip wound on a form of about 1.7 *cm* radius and pitch of 2.43 *cm*.

After complete assembly of the Pierce gun and microwave circuit, the tube was aligned. A rough alignment was made using magnetic axis measurements, then fine adjustments were made by bolts attached to the mounting fixture and monitored by means of micrometers. Because of the magnetic material integral to the Pierce gun and the large magnetic field from the superconducting magnet, substantial axial compressive forces on the gun existed. As a result, the gun was not free to follow adjustments to the output end of the tube, and flexure of the vacuum envelope ocurred. Consequently, tube movement was avoided after initial alignment was compete.

The dispersion diagram for the BWO is shown in Fig. 4. The curve

is the cavity dispersion relation, given by

$$\omega^2 = k_{\|}^2 c^2 + \omega_c^2 \ , \tag{1}$$

where ω and ω_c are the oscillating and cutoff frquencies respectively, and $k_{\|}$ is the parallel wavenumber component. The line is the Doppler shifted frequency of the oscillating mode given by

$$\omega = k_{\|} v_{\|} + \Omega_{ce} \ , \tag{2}$$

where $v_{\|}$ is the parallel beam velocity. For the BWO cavity, radius $r_c = .214\ cm$, length $2.14\ cm$, the cutoff frequencies for some of the modes near the design mode $TE_{1,2}$, are given in Table I.

Table I.

Mode	Bessel zero	$\omega_c/2\pi$ (GHz)
$TE_{1,1}$	1.84118	41.03
$TE_{2,1}$	3.05424	68.07
$TE_{0,1}$	3.83171	85.39
$TE_{1,2}$	5.33144	118.81
$TE_{2,2}$	6.70613	149.45
$TE_{0,2}$	7.01559	156.35

The design mode is just below the $TE_{2,2}$ and $TE_{0,2}$ cutoff frequencies, and these two modes are closely spaced.

Initial radiation results from the BWO-gyrotron were at frequencies that were slightly above the cavity cyclotron frequency and corresponded to forward modes. From frequency measurements, these modes were identified as $TE_{2,2}$ and $TE_{0,2}$ modes and frequencies about 150 GHz and 158 GHz respectively. Varius cavity magnetic fields and beam voltages were used with no evidence of the backward wave. All of this operation used a blank fused sillica widow rather than the moth-eye window.

Later, additional magnet strips were added to the wiggler bringing the transverse field to about 18 G (Fig. 5). Forward waves were again

observed for this case, however, the backward wave was also observed. The blank window was still in place for this series of experiments. Figure 6 shows the frequency ratio ω_o/Ω_e, where ω_o and Ω_e are the observed and the cavity electron cyclotron frequency, as a function of the observed frequency. The backward wave measurements have $\omega_o/\Omega_e < 1$ and have frequency in the range 133 GHz to 143 GHz which is approximately that of the original design. One of the characteristics of the BWO is that it is voltage tunable. Results of voltage scans are shown in Fig. 7 as a function of two of the operating parameters, the wiggler axial field (abcissa) and the cathode voltage (ordinate). The data indicate the location and frequency of observed oscillations. Both forward and backward waves are included. The resonance for electrons in the wiggler is shown as a solid line and is given by

$$\Omega_{we} = \frac{v_z}{p_w} , \tag{3}$$

where Ω_{we}, $v_z \approx c\beta$, and p_w are the electron cyclotron frequency in the wiggler axial field, the beam velocity, and the wiggler period. Equivalently,

$$B_{zw} = \frac{\gamma m_o c^2}{e} k_w \beta_z . \tag{4}$$

The axial field at the wiggler is B_{zw}, $k_w = 2\pi/p_w$, and β_z is the normalized beam velocity. As indicated by the discrete points in the figure, the voltage tuning was not continuous with the beam voltage. For a given resonance in the wiggler and constant velocity ratio, the backward wave frequency appeared at successive seperated voltage intervals. The frequencies have the proper scaling given by

$$\frac{\partial \omega_b}{\partial V_c} = \frac{e(\omega_b - \Omega_e)}{\gamma m_o c^2} \left(\frac{1}{\beta_{||}^2} - 1 \right) < 0 . \tag{5}$$

Near the boundry of backward and forward wave operation, both modes could occassionally be observed simultaneously. Multi-mode operation with

several backward modes was also ocassionally observed for parameters near the center of the BWO operation region.

The emitted power was monitored by a calorimeter placed just outside the window. For the forward modes, power as high as $\approx 4.5\ kW$ was observed. The power for the backward waves was $\leq 1\ kW$ for efficiencies of $\approx .5\%$.

The resonance condition for the electrons in the wiggler, Eqns, (3), and (4), show a multi-parameter dependence of the perpendicular energy. The net result can be determined by monitoring the velocity ratio α at or near the interaction region. One methode of determining α is to solve Eqns. (1)and (2) to get

$$\beta_{\parallel} = \frac{\frac{\Omega_{ce}}{\omega} - 1}{\sqrt{1 - \left(\frac{\omega_c}{\omega}\right)^2}} \ . \tag{6}$$

Calculation of the voltage depression for a solid beam in the interaction region requires only knowledge of I_b and the average parallel beam velocity and is given by

$$\delta V \approx \frac{I_b \mu_o c^2}{4\pi \langle v_{\parallel} \rangle} \left(1 + 2\, ln\left(\frac{r_c}{r_b}\right)\right) \ , \tag{7}$$

where r_c, r_b are the cavity and beam radius respectively. Then

$$\langle \beta_{\perp} \rangle = \sqrt{1 - \frac{1}{\gamma'^2} - \langle \beta_{\parallel} \rangle^2} \tag{8}$$

with

$$\gamma' = 1 + \frac{e(V_c - \delta V)}{m_o c^2} \ . \tag{9}$$

The desired result is $\langle \alpha \rangle = \langle \beta_{\perp} \rangle / \langle \beta_{\parallel} \rangle$. Figure 8 shows the α values calculated using this technique. Velocity ratios fall between 1.5 and 6.5. Those

points at higher frequency have a large uncertainty because of the small differences between the observed, cyclotron and cutoff frequencies. A capacitance probe was also installed in the beam tunnel near the entrance to the interaction region, however, the velocity ratio values had large uncertainty because of low signal level and noise pickup.

In summary, backward wave operation has been observed over a relatively wide range of frequencies ($133 - 143\ GHz$) at low power ($\leq 1\ kW$) with low effiency ($\leq .5\%$). Voltage tuning of the frequency has been demonstrated, however, it is not continuous and occassionally multi-mode operation is observed.

Status and Future Plans

The BWO gyrotron has been removed from the superconducting magnet and partially disassembled for storage. Several design changes are anticipated before reassembly and operation.

- Increase radius of vacuum envelope at the beam tunnel. An annular space around the outside of the beam tunnel will allow increased pumping of the gun region by the collector vacuum pump.
- Conduct experiments using moth-eye window. It will be mounted after alignment with the fused silica window.
- Redesign cavity and uptaper by making the cavity slightly shorter and adding a non-linear taper at the cavity exit aperature. Multi-mode oscillations may be a result of interactions extending into the uptaper.
- Redesign capacitive probe to take advantage of design improvements from the megawatt tube.

These improvements address the problems observed in the initial operation of the tube should mitigate them.

References

[1]D.R. Pirkle, C.W. Alvord, M.H. Anderson, R.F. Garcia, and A.L. Nordquist, *IEDM Tech. Digest* p. 159, 1988

[2]S.Y. Park, R.H. Kyser, C.M. Armstrong, and R.K. Parker, *International Electron Devices Meeting Technical Digest*, Washington, D.C., Dec. 6-9, 1987, p. 933

Figure Captions

Figure 1. Schematic of the BWO-gyrotron system. The electron beam travels from the Pierce gun through the wiggler then to the cavity at the superconducting field maximum and ends on the collector.

Figure 2. The relative position of the superconductor and wrap-on magnets was adjusted so that the axial magnetic field was monotonicaly decreasing from the cavity. Length measurements are with respect to the superconductor magnetic field maximum.

Figure 3. Transverse field components, and total transverse field for two layers of magnet material.

Figure 4. Dispersion diagram for the BWO cavity. Abcissa and ordinate are normalized to $k_{\perp 11}$ and ω_{c11}, the cutoff wavenumber and frequency, for the $TE_{1,1}$ mode.

Figure 5. Transverse field components, and total transverse field for five layers of magnet material.

Figure 6. Observed frequency ω_o normalized by the electron cyclotron frequency Ω_e as a function of observed frequency.

Figure 7. Observed operating points and their frequencies as a function of wiggler axial field (abcissa) and cathode voltage (ordinate). Forward and backward waves are included. The solid line is the wiggler resonance given by $\Omega_{we} = v_b/p_w$.

Figure 8. Average alpha as a function of oscillator frequency.

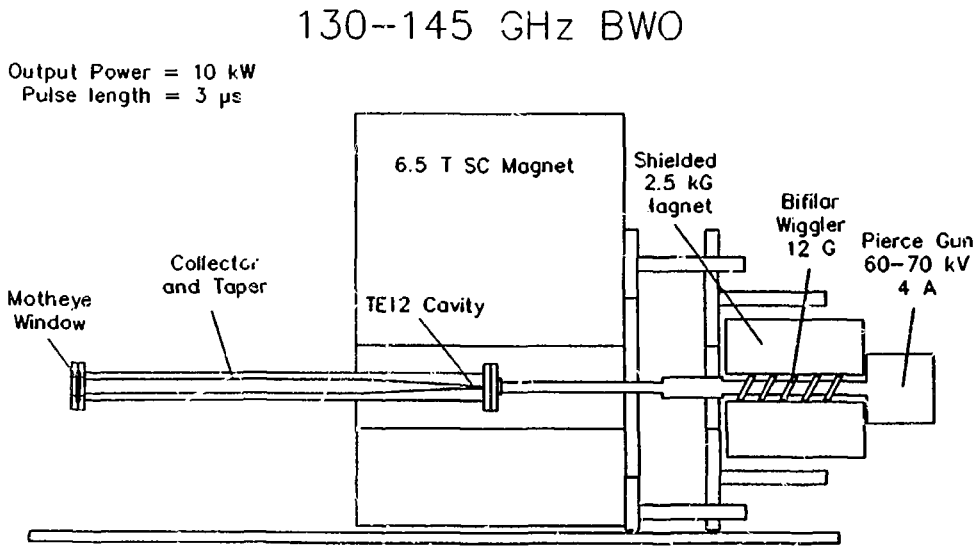
130--145 GHz BWO
Output Power = 10 kW
Pulse length = 3 μs
6.5 T SC Magnet
Shielded
2.5 kG
Magnet
Bifilar
Wiggler
12 G
Pierce Gun
60-70 kV
4 A
Collector
and Taper
Motheye
Window
TE12 Cavity

Figure 1

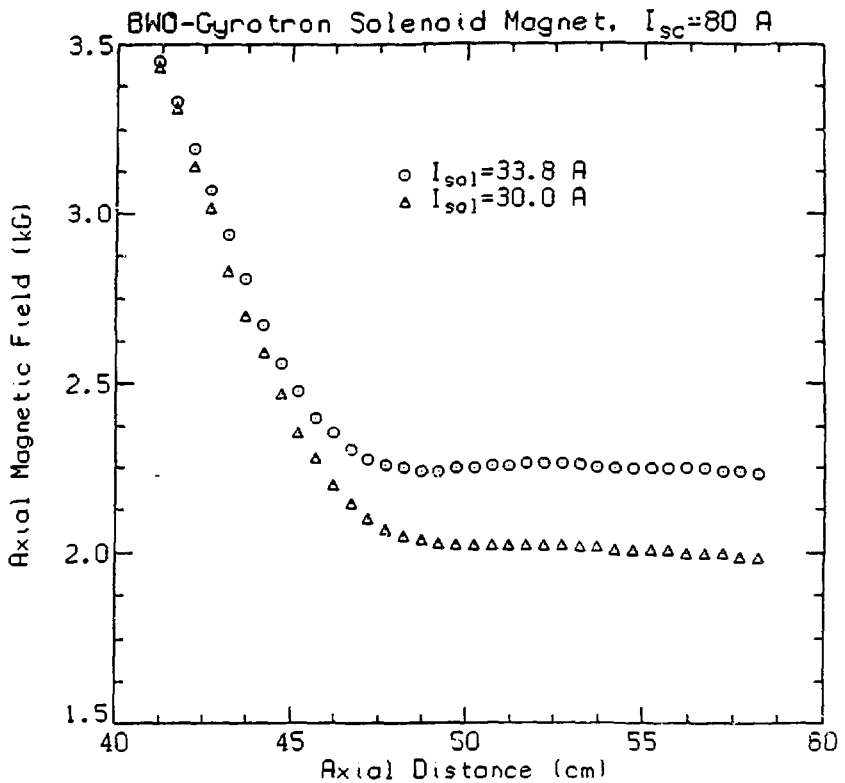
BWO-Gyrotron Solenoid Magnet, I_{sc}=80 A
I_{sol}=33.8 A
I_{sol}=30.0 A
Axial Magnetic Field (kG)
Axial Distance (cm)
3.5
3.0
2.5
2.0
1.5
40
45
50
55
60

Figure 2

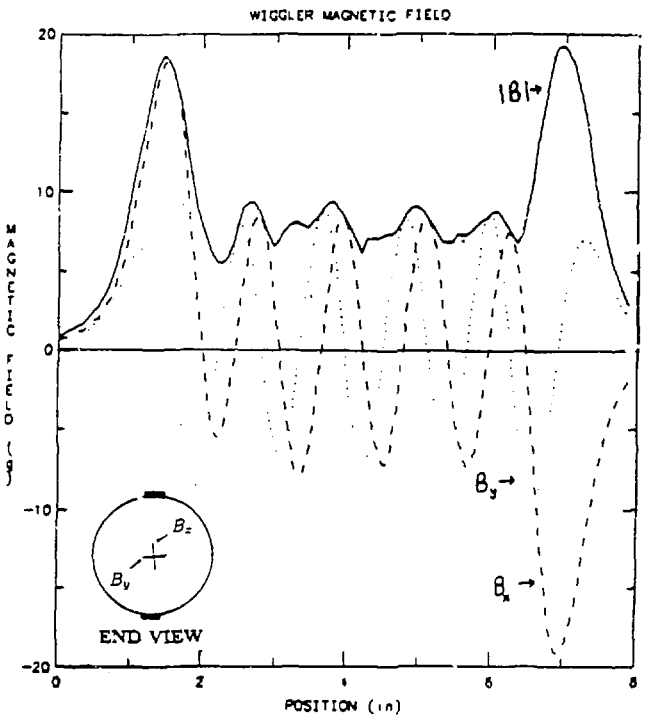
WIGGLER MAGNETIC FIELD
20
10
0
-10
-20
MAGNETIC FIELD (kG)
|B|→
B_y→
B_x→
B_z
B_y
END VIEW
0
2
4
6
8
POSITION (in)

Figure 3

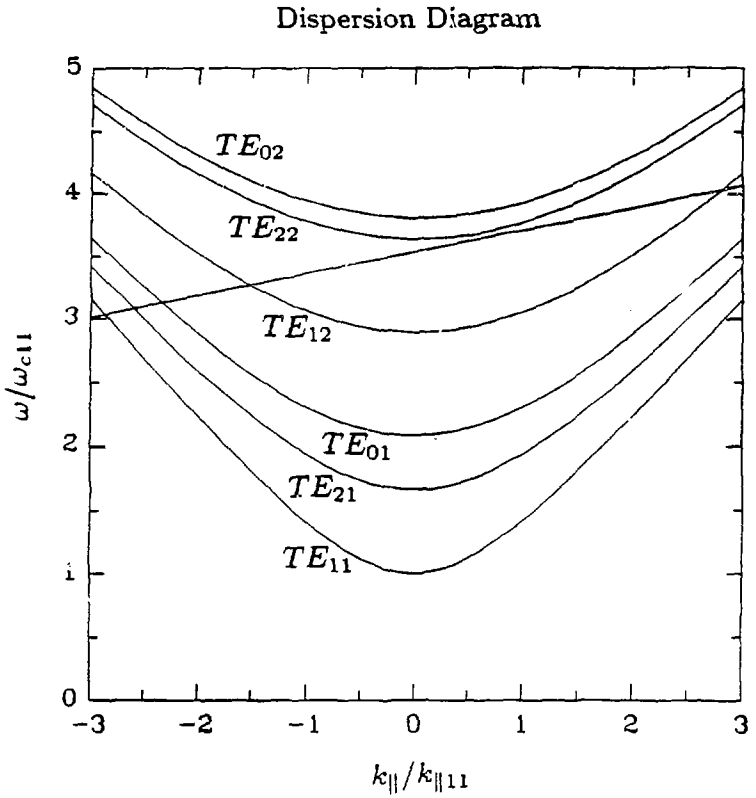
Dispersion Diagram
5
4
3
2
1
0
ω/ω_{c11}
TE_{02}
TE_{22}
TE_{12}
TE_{01}
TE_{21}
TE_{11}
−3
−2
−1
0
1
2
3
$k_{\parallel}/k_{\parallel 11}$

Figure 4

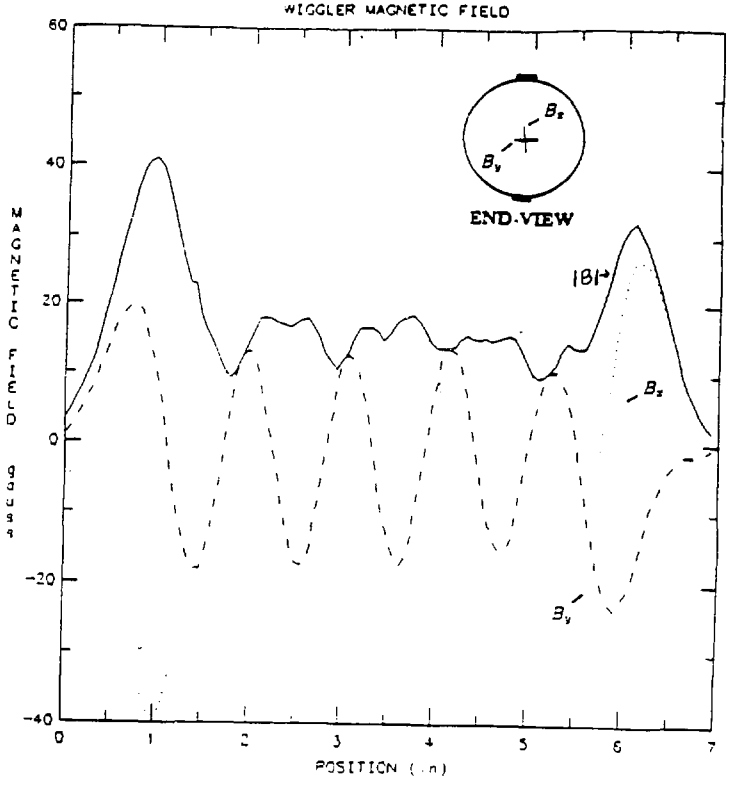
WIGGLER MAGNETIC FIELD
60
40
20
0
-20
-40
MAGNETIC FIELD gauss
0
1
2
3
4
5
6
7
POSITION (m)
B_z
B_y
END-VIEW
|B|
B_z
B_y

Figure 5

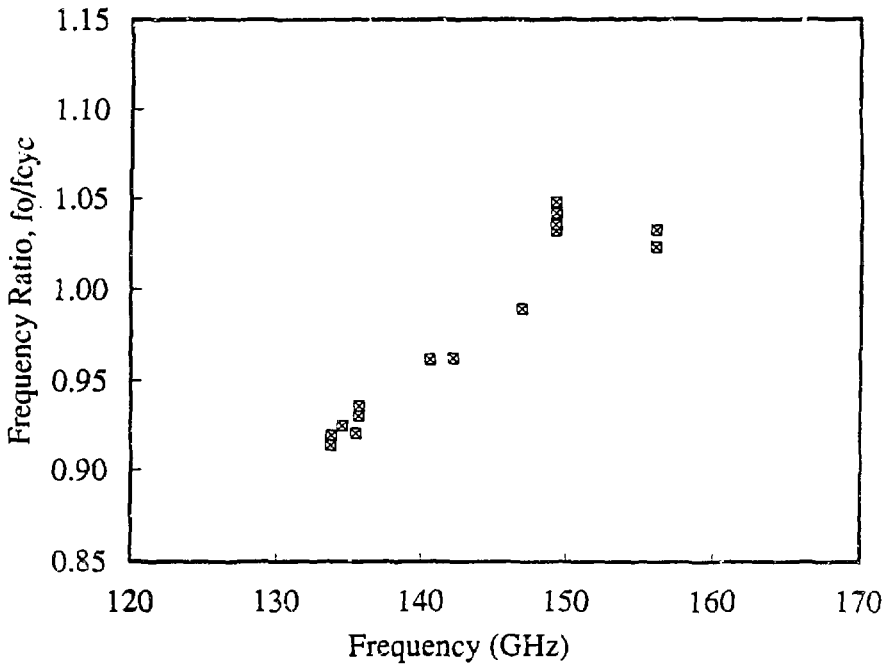
1.15
1.10
1.05
1.00
0.95
0.90
0.85
Frequency Ratio, fo/fcyc
120
130
140
150
160
170
Frequency (GHz)

Figure 6

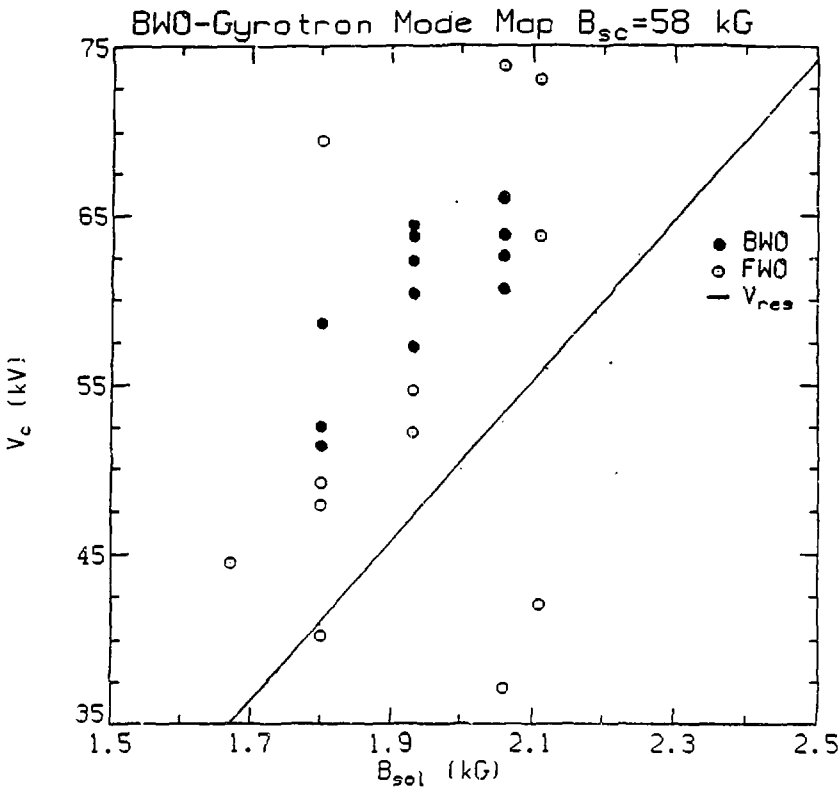
BWO-Gyrotron Mode Map B_{sc}=58 kG
75
65
55
45
35
V_c (kV)
1.5
1.7
1.9
2.1
2.3
2.5
B_{sol} (kG)
BWO
FWO
V_{res}

Figure 7

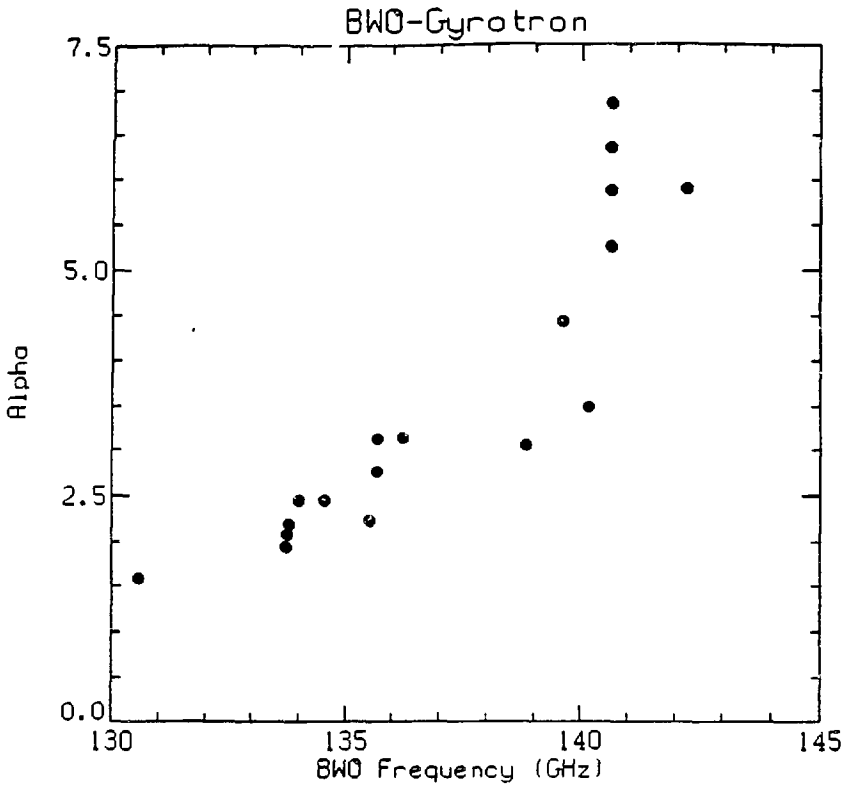
BWO-Gyrotron
7.5
5.0
2.5
0.0
Alpha
130
135
140
145
BWO Frequency (GHz)

Figure 8